

Applicability and Limitations of Quantum Circuit Cutting in Classical State-Vector Simulation

Mitsuhiro Matsumoto,^{1,*} Shinichiro Sanji,¹ and Takahiko Satoh²

¹*Technology Laboratory, PwC Consulting LLC, Japan*

²*Faculty of Science and Technology, Keio University, Japan*

Circuit cutting partitions a large quantum circuit into smaller subcircuits that can be executed independently and recombined by classical post-processing. In classical state-vector simulation with full-state reconstruction, the runtime is governed by a trade-off between reduced subcircuit size and the overheads of exponentially many subcircuits and full-state reconstruction. For equal partitioning, we derive threshold conditions on the number of cuts below which cutting reduces the wall-clock time. State-vector experiments validate the predicted speedup boundary up to 24 qubits, and a runtime breakdown up to 30 qubits identifies crossovers at $q \approx 18$ and $q \approx 22$ where merging overtakes first preprocessing and then subcircuit simulation. As a practical guideline, we show that under a 10-minute wall-clock budget, two-way cutting extends the maximum feasible qubit count by 4 to 6 qubits relative to simulation without cutting.

I. INTRODUCTION

Quantum computing holds the potential to exponentially outperform classical computing for specific computational problems [1]. However, current Noisy Intermediate-Scale Quantum (NISQ) devices remain severely constrained by the number and quality of available qubits [2]. To overcome these limitations, circuit cutting, a technique that partitions large quantum circuits into smaller subcircuits for independent execution, has emerged as an approach to extend the effective circuit size beyond near-term device limits [3–5].

Existing research on circuit cutting has focused on minimizing the overhead associated with partitioning [6, 7]. On the classical simulation side, hybrid Schrödinger–Feynman methods [8] and tensor-network-based approaches [9, 10] exploit circuit partitioning to push simulation beyond naive memory limits, and the fundamental trade-off between partition size and the exponential growth of subcircuit count is well recognized. Classical simulation remains indispensable for verification, benchmarking, and workflow-level performance studies of quantum algorithms, especially when end-to-end runtime is the quantity of interest. However, under concrete execution pipelines for classical state-vector simulation with full-state reconstruction, the cut count at which end-to-end wall-clock overhead outweighs the reduced subcircuit size has received limited attention. A closed-form guideline for the cut threshold would help allocate finite classical resources and clarify when cutting is practically beneficial in wall-clock time.

Relatedly, circuit cutting has been studied as a workflow that distributes a large circuit into subcircuits and recombines them by classical post-processing [11]. The practical classical simulation frontier is likewise shaped by high-performance state-vector simulators [12–14],

tensor-network backends [15], and large-scale partitioning demonstrations [16]. These developments motivate an end-to-end wall-clock analysis of circuit cutting, which is the focus of this paper.

This work focuses on classical state-vector simulation with full-state reconstruction, arising in benchmarking, debugging, and verification of quantum devices. Cutting reduces the subcircuit size but exponentially increases the number of subcircuits, and in this setting the results must be combined into the full 2^q -dimensional state vector at an additional $O(2^q)$ merging cost. Judging whether cutting is beneficial therefore requires an end-to-end wall-clock analysis covering all stages of the cutting workflow. To our knowledge, a quantitative wall-clock analysis under this specific setting has not been systematically reported.

We analyze the wall-clock efficiency of circuit cutting in classical state-vector simulation, presenting three main contributions:

First, we decompose the total cutting time into preprocessing, subcircuit simulation, and merging, and analyze their relative scaling. This reveals two bottleneck crossovers as qubit count increases: merging surpasses preprocessing and surpasses subcircuit simulation. In our implementation, these crossovers appear at intermediate qubit counts (around $q \approx 18$ and $q \approx 22$ in our setup). Second, from this cost model we derive conditions on the maximum total cut count c_{total} for which cutting yields a net speedup under equal partitioning into n segments. The threshold takes the form $c_{\text{total}} \propto q$ and is approximately depth-independent. State-vector experiments up to 24 qubits confirm the predicted threshold.

Third, under a 10-minute wall-clock budget, two-way cutting extends the maximum feasible qubit count by 4 to 6 qubits compared to simulation without cutting, with the gain increasing at larger depths.

We begin by reviewing circuit cutting methods and their computational characteristics in Sec. II. We introduce the execution time model and its regime structure in Sec. III, and derive cut-threshold conditions for equal

* mitsuhiro.matsumoto@pwc.com

partitioning into n segments in Sec. IV. We present numerical results and confirm the predicted trends using classical state-vector simulations in Sec. V. Finally, we summarize our findings and conclude in Sec. VI.

II. BACKGROUND

A. Circuit cutting

Circuit cutting decomposes a large circuit into an ensemble of smaller subcircuits whose outcomes are recombined by classical post-processing. In practice, two representative approaches are (i) *wire cutting* (cutting “wires” by inserting measure-and-prepare channels) and (ii) *gate cutting* (replacing non-local entangling gates across partitions with decomposed local operations). This work focuses on gate cutting in the classical state-vector setting, whose overhead structure differs qualitatively from the hardware setting.

1. Quantum hardware setting

On quantum hardware, circuit cutting incurs a sampling overhead that grows exponentially with the number of cut locations. For gate cutting, each non-local gate is replaced by a quasiprobability decomposition (QPD) into local channels [5]. Optimal sampling overheads for cutting multiple two-qubit unitaries have been characterized [17]. For wire cutting, qubit wires are severed by inserting measure-and-prepare channels [4]. The sampling cost scales as $\tilde{\mathcal{O}}(4^m/\epsilon^2)$ for cutting m parallel wires (up to polylog factors), with an information-theoretic lower bound of $\Omega(2^m/\epsilon^2)$ [18]. Recent works study wire-cutting schemes that achieve optimal or near-optimal overheads under different operational constraints such as ancilla usage [6, 7].

2. Classical state-vector setting

When subcircuits are simulated classically via state-vector simulation, a different decomposition is available. Any two-qubit unitary U admits an operator-Schmidt decomposition [19]

$$U = \sum_{\ell=1}^k s_{\ell} (A_{\ell} \otimes B_{\ell}), \quad (1)$$

where A_{ℓ} and B_{ℓ} are single-qubit operators, s_{ℓ} are complex coefficients, and k is the Schmidt rank of U . For two-qubit gates, the Schmidt rank takes only the values $k = 2$ (controlled unitaries such as CZ and CX) or $k = 4$ (all other non-local gates such as SWAP) [19].

Because the classical simulator has direct access to the full state vector, the linearity of Eq. (1) can be exploited

directly: each term produces an independent subcircuit state vector, and the results are summed as complex vectors. This yields k terms per cut, with no sampling overhead.

For example, the CZ gate ($k = 2$) admits the decomposition [20]

$$\text{CZ} = \frac{1}{1+i} (S \otimes S + i S^{\dagger} \otimes S^{\dagger}), \quad (2)$$

where $S = \text{diag}(1, i)$ is the phase gate. Each term is a tensor product of single-qubit unitaries, so cutting one CZ gate at a partition boundary replaces it with two subcircuits that apply S or S^{\dagger} to the respective segments. The CX gate is related by $\text{CX} = (I \otimes H) \text{CZ} (I \otimes H)$ and admits the same two-term decomposition up to local basis changes. When c gates are cut, the number of subcircuits grows as k^c (exponentially with the number of cuts).

B. Classical simulation

Schrödinger-style (state-vector) simulation stores a state vector of size 2^q for a q -qubit system. This exponential memory footprint quickly becomes the primary bottleneck. A well-known reference point is the “49-qubit barrier”, which motivated decomposition/slicing and storage-aware strategies to push exact simulation beyond naive memory limits [10]. Beyond exact simulation, approximate approaches deliberately trade accuracy for scale. One direction is *lossy state-vector compression*, e.g., quantization- or compression-based methods that reduce bits per amplitude while controlling the induced error/fidelity loss [21, 22]. Another direction is approximate generation of samples at a *target fidelity* for structured benchmarks (e.g. Sycamore-style random circuits), which provides scalable classical baselines without computing the full exact state [9].

Tensor-network simulators [23] can be more effective than state-vector simulation for circuits with favorable structure such as limited entanglement or small treewidth. Several large-scale approximate sampling results can also be phrased naturally in tensor-network terms. Here we focus on the state-vector regime and quantify when circuit cutting reduces *classical wall-clock runtime* by trading reduced subcircuit size for cutting overhead.

III. EXECUTION TIME MODEL

We model the wall-clock time of circuit cutting on a single compute node with sequential subcircuit execution, without gate fusion or parallelization. Because the cutting and recombination procedure in the classical state-vector setting exactly recovers the full state vector of the uncut circuit (up to machine precision), fidelity loss

does not arise and we focus exclusively on the execution-time trade-off.

A. Definitions and cost decomposition

To evaluate whether circuit cutting reduces the classical simulation time, we decompose the total cutting time as

$$T_{\text{cut}} = T_{\text{pre}} + T_{\text{sub}} + T_{\text{merge}}, \quad (3)$$

where T_{pre} is the preprocessing time for generating all subcircuits and associated coefficients, $T_{\text{sub}} = \sum_{i=1}^{N_{\text{sub}}} T_{\text{SV}}^{(i)}$ is the total subcircuit simulation time ($T_{\text{SV}}^{(i)}$ is the state-vector simulation time of the i -th subcircuit), and T_{merge} is the merging time to reconstruct the full state vector by combining subcircuit outcomes. The baseline for comparison is $T_{\text{orig}} = O(2^q D)$, the wall-clock time of simulating the original circuit without cutting.

We consider a circuit on q qubits partitioned into n segments. Let c_i denote the total number of gate cuts on all boundaries adjacent to segment i , q_i the number of qubits in segment i , and $c_{\text{max}} = \max_i c_i$. The total number of subcircuits is $N_{\text{sub}} = \sum_{i=1}^n k^{c_i}$, where k is the Schmidt rank of the cut gates.

The computational cost of each phase scales as shown in Table I. Here D denotes the depth of the original circuit and $D_{\text{seg},i} (\leq D)$ denotes the depth of segment i after partitioning. We write $D_{\text{seg}} = \max_i D_{\text{seg},i}$. Because gate fusion is not applied, the lower bound $D_{\text{seg}} \geq D/n$ is approached when gates are distributed uniformly across segments, giving

$$\frac{D}{n} \leq D_{\text{seg}} \leq D. \quad (4)$$

The preprocessing phase generates all N_{sub} subcircuits by traversing the original circuit once per subcircuit. Each subcircuit simulation operates on a reduced state vector of 2^{q_i} amplitudes, but must be repeated for all N_{sub} terms. The merging phase reconstructs the full 2^q -dimensional state vector by summing $k^{c_{\text{max}}}$ tensor products. The memory cost of subcircuit simulation is $O(2^{q_{\text{max}}})$ if state vectors are discarded after each subcircuit, or $O(N_{\text{sub}} \cdot 2^{q_{\text{max}}})$ if all are retained simultaneously, where $q_{\text{max}} = \max_i q_i$. The pseudocodes for each phase are given in Appendix B.

B. Regime structure of the cutting cost

The three cost components in Eq. (3) exhibit qualitatively different dependences on the circuit parameters. To identify which component dominates T_{cut} , we compare the three components using their scaling from Table I.

To obtain closed-form ratio expressions, we now specialize to equal partitioning ($q_i = q/n$ for all i , $D_{\text{seg},i} = D_{\text{seg}}$ for all i).

TABLE I. Computational cost summary. q : total qubits, n : segments, c_i : number of cuts adjacent to segment i , $c_{\text{max}} = \max_i c_i$, k : Schmidt rank of the cut gate, D : original circuit depth, D_{seg} : maximum subcircuit depth, $N_{\text{sub}} = \sum_i k^{c_i}$: total number of subcircuits.

Phase	Time	Memory
Preprocessing	$O(N_{\text{sub}} D)$	$O(N_{\text{sub}} D)$
Subcircuit sim.	$O(N_{\text{sub}} 2^{q_{\text{max}}} D_{\text{seg}})$	$O(2^{q_{\text{max}}})$
Merging	$O(k^{c_{\text{max}}} 2^q)$	$O(2^q)$

1. T_{pre} vs T_{sub}

From Table I,

$$\frac{T_{\text{pre}}}{T_{\text{sub}}} = \frac{D}{2^{q/n} D_{\text{seg}}}. \quad (5)$$

This ratio is independent of k and c_i . From Eq. (4),

$$\frac{1}{2^{q/n}} \leq \frac{T_{\text{pre}}}{T_{\text{sub}}} \leq \frac{n}{2^{q/n}}. \quad (6)$$

Since $2 \leq n \leq q$ and $2^{q/n} \geq 2$, the upper bound $n/2^{q/n}$ vanishes as q/n grows, so $T_{\text{pre}} \ll T_{\text{sub}}$ holds whenever q/n is sufficiently large. For small q/n (e.g. $q/n \lesssim 5$), the two can be comparable.

2. T_{pre} vs T_{merge}

From Table I,

$$\frac{T_{\text{pre}}}{T_{\text{merge}}} = \frac{N_{\text{sub}}}{k^{c_{\text{max}}}} \cdot \frac{D}{2^q}. \quad (7)$$

The first factor satisfies

$$\frac{N_{\text{sub}}}{k^{c_{\text{max}}}} = \sum_{i=1}^n k^{c_i - c_{\text{max}}} \leq n, \quad (8)$$

since each term $k^{c_i - c_{\text{max}}} \leq 1$. The bound is saturated when all segments share the same number of cuts and decreases toward unity as the cut distribution becomes more uneven. In either case, this factor is $O(n)$ and does not introduce exponential dependence on q or c . The ratio is therefore controlled by $D/2^q$. When $2^q \gg D$, $T_{\text{pre}} \ll T_{\text{merge}}$ holds regardless of n . For small q or very deep circuits where D and 2^q are comparable, T_{pre} can be comparable to T_{merge} . Combined with the result of Sec. III B 1, T_{pre} is the smallest component of T_{cut} whenever q/n and q are both sufficiently large.

3. T_{sub} vs T_{merge}

From Table I,

$$\frac{T_{\text{sub}}}{T_{\text{merge}}} = \frac{N_{\text{sub}}}{k^{c_{\text{max}}}} \cdot \frac{D_{\text{seg}}}{2^{q(1-1/n)}}. \quad (9)$$

The first factor is $O(n)$ by Eq. (8). The regime boundary is therefore governed by

$$\frac{D_{\text{seg}}}{2^{q(1-1/n)}} \approx 1. \quad (10)$$

When $D_{\text{seg}} \gg 2^{q(1-1/n)}$ (small q or large D_{seg}), T_{sub} dominates T_{cut} (subcircuit-dominant regime). In the opposite limit $D_{\text{seg}} \ll 2^{q(1-1/n)}$ (large q or small D_{seg}), T_{merge} dominates (merge-dominant regime).

4. Crossover structure

The preceding ratios imply that, at fixed depth, increasing q drives two crossovers: T_{merge} overtakes T_{pre} and T_{sub} . Once T_{merge} overtakes both, it is the dominant component of T_{cut} . Since T_{merge} does not benefit from the reduced subcircuit size, the advantage of cutting is limited in this regime. In Sec. IV, we apply this cost model to derive quantitative threshold conditions, which are then verified by wall-clock measurements in Sec. V.

IV. THRESHOLD ANALYSIS

We derive conditions on the number of cuts under which circuit cutting reduces the classical simulation time. We consider a circuit on q qubits with depth D , partitioned into n equal segments of q/n qubits each, with c cuts per boundary and $c_{\text{total}} = c(n-1)$ cuts in total. We assume that gates are distributed uniformly across segments, so that each subcircuit has depth $D_{\text{seg}} \approx D/n$.

A. Cost comparison framework

The total cutting time $T_{\text{cut}} = T_{\text{pre}} + T_{\text{sub}} + T_{\text{merge}}$ has three components whose scaling is given in Table I. Of these, T_{pre} is never the dominant component. The ratio analysis in Sec. IIIB shows that $T_{\text{pre}}/T_{\text{sub}}$ and $T_{\text{pre}}/T_{\text{merge}}$ both decrease with q , and the runtime breakdown in Sec. VC confirms that T_{pre} never dominates T_{cut} in any tested configuration. We therefore omit T_{pre} from the threshold analysis.

The remaining two components involve qualitatively different operations. T_{sub} and T_{orig} both perform gate-by-gate state-vector simulation using the same simulator, differing only in the size of the state vector and the number of gates. These differences are already captured by the explicit factors $2^{q/n}$ and D_{seg} in Table I, so the order-of-magnitude comparison T_{sub} vs. T_{orig} is reliable. We derive the threshold from this pair. In contrast, T_{merge} performs vectorized tensor products and vector additions, which are a different type of computation from gate-by-gate simulation. The relative cost of these two types of operations depends on the implementation and is not

captured by the $O(\cdot)$ scaling. T_{merge} is therefore not included in the theoretical threshold, but is accounted for in the empirical evaluation.

B. Threshold for equal partitioning

1. Threshold under uniform gate distribution

Under the equal-partitioning setup of this section, comparing T_{sub} and T_{orig} from Table I,

$$N_{\text{sub}} \cdot 2^{q/n} \cdot \frac{D}{n} < 2^q \cdot D, \quad (11)$$

which simplifies to

$$\frac{N_{\text{sub}}}{n} < 2^{q(1-1/n)}. \quad (12)$$

The depth D cancels, so this condition depends only on q , n , c , and k .

We now set $k = 2$ (CZ gate cutting) and derive explicit thresholds.

a. Bipartite case ($n = 2$). With $N_{\text{sub}} = 2 \cdot 2^{c_{\text{total}}}$, Eq. (12) gives

$$c_{\text{total}} < \frac{q}{2}. \quad (13)$$

b. General $n \geq 3$. The interior term dominates in N_{sub} , giving $N_{\text{sub}} \approx (n-2) \cdot 2^{2c_{\text{total}}/(n-1)}$. Substituting into Eq. (12) and taking logarithms gives

$$c_{\text{total}} < \frac{q(n-1)^2}{2n} + \frac{(n-1) \log_2 \left(\frac{n}{n-2} \right)}{2}. \quad (14)$$

The leading slope in the (q, c_{total}) plane is $(n-1)^2/(2n)$, which increases with n . We denote the second term in Eq. (14) by δ . For practically relevant values of n (up to about 10), δ remains close to 1.5.

Table II summarizes the threshold parameters for $n = 2, 3$, and 4. These thresholds guarantee $T_{\text{sub}} < T_{\text{orig}}$ and provide a practical guideline for selecting the number of cuts. The additional contribution of T_{merge} , which grows as $O(k^{c_{\text{max}}} \cdot 2^q)$, is not included in these thresholds and can become significant at large q .

TABLE II. Subcircuit-simulation threshold $c_{\text{total}} < c_{\text{total}}^{\text{max}}$ for $k = 2$ (CZ gate cutting). The threshold has the form $c_{\text{total}} < \text{slope} \times q + \delta$. These conditions compare T_{sub} with T_{orig} and do not include T_{merge} .

n	Slope	δ
2	1/2	0
3	2/3	$\log_2 3 \approx 1.58$
4	9/8	3/2

2. Effect of non-uniform gate distribution

When gates are not distributed uniformly across segments, some subcircuits contain more gates than others, resulting in $D_{\text{seg}} > D/n$. For general D_{seg} , the condition $T_{\text{sub}} < T_{\text{orig}}$ becomes

$$\frac{N_{\text{sub}}}{2^{q(1-1/n)}} \cdot \frac{D_{\text{seg}}}{D} < 1. \quad (15)$$

Since $D/n \leq D_{\text{seg}} \leq D$, the second factor D_{seg}/D ranges from $1/n$ (uniform) to 1 (worst case). For $n = 2$, the c_{total} threshold decreases by 1 cut compared with Eq. (13). For $n \geq 3$, the reduction is $(n-1) \log_2(n)/2$, which equals 1.6 for $n = 3$ and 3.0 for $n = 4$. The uniform-depth threshold represents the most favorable case. The reduction is modest for small n but grows with n , so for large n the actual gate distribution should be taken into account.

The thresholds derived in this section compare T_{sub} with T_{orig} and do not include T_{merge} . The contribution of T_{merge} to the total cutting time is quantified empirically in Sec. V C.

V. EVALUATION

We verify the threshold conditions on a classical state-vector simulator and report a runtime breakdown.

A. Experimental setup

1. Simulation environment

All experiments were performed on a single compute node (Apple M3 Max, 128 GB RAM) running Python 3.10.8 and Qiskit 2.2.3. State-vector simulation was carried out using the `Statevector` class (`qiskit.quantum.info`). We report wall-clock time measured on the same machine for all runs. For the runtime breakdown measurements (Fig. 3), memory was explicitly freed between runs to avoid growth in the pre-processing time at large qubit counts. Unless stated otherwise, each configuration was measured ten times, and we report the mean values.

2. Circuit family and partitioning

We use a synthetic circuit family for threshold validation. A representative instance is shown in Fig. 1. For two or more cuts, the circuit is extended by appending additional copies of this circuit after removing the initial Hadamard gates. This repeated-block structure, alternating single-qubit and two-qubit gate layers, mirrors the layout of practical variational and simulation circuits, such as Ansätze used in VQE [24, 25], QAOA circuits [26], and Trotterized Hamiltonian simulation [27].

In all of these, increasing the number of repeated layers simultaneously increases both the circuit depth and the number of two-qubit gates across partition boundaries.

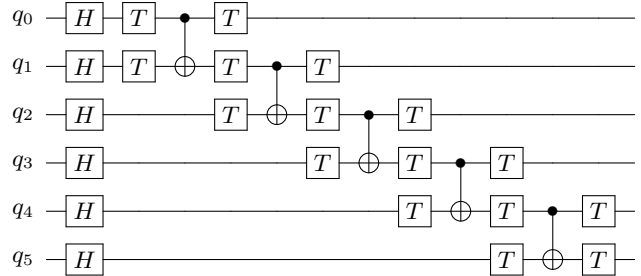


FIG. 1. An original circuit which we can partition by one cut. For two or more cuts, the circuit is extended by appending additional copies of this circuit after removing the initial Hadamard gates.

We use equal partitioning into n subcircuits with q/n qubits each, since it minimizes the simulation time, as confirmed in Appendix A 1. All experiments in the remainder of this section use equal partitioning.

3. Runtime measurement and evaluation

We measure T_{cut} and its three components T_{pre} , T_{sub} , and T_{merge} as defined in Eq. (3). For each combination of (q, c_{total}) , we evaluate the relative speedup

$$\Delta = (T_{\text{cut}} - T_{\text{orig}})/T_{\text{orig}}, \quad (16)$$

where $\Delta < 0$ indicates a speedup.

B. Validation of threshold conditions

Using the experimental setup described in Sec. V A, the heat maps in Fig. 2 show the relative speedup Δ on the (q, c_{total}) plane for $n = 2$ and $n = 3$. In both cases, the boundary between the speedup region ($\Delta < 0$, blue) and the slowdown region ($\Delta > 0$, red) broadly follows the theoretical thresholds derived in Sec. IV.

To quantify the measured boundary, we fit a linear decision boundary to each panel using a weighted support vector machine (SVM) classifier, indicated by the solid line in Fig. 2. The SVM-fitted boundaries are $c_{\text{total}} = 0.70q - 7.30$ ($n = 2$) and $c_{\text{total}} = 1.00q - 11.50$ ($n = 3$), while the theoretical thresholds, Eqs. (13) and (14), are $c_{\text{total}} < q/2$ ($n = 2$) and $c_{\text{total}} < 2q/3 + \log_2 3$ ($n = 3$). Comparing the two, the measured boundary has a steeper slope and a more negative intercept.

This discrepancy arises because the theoretical threshold compares only T_{sub} with T_{orig} , omitting T_{pre} and T_{merge} . In the benchmark circuit, depth D increases with c_{total} . Since $T_{\text{merge}} = O(k^{c_{\text{max}}} \cdot 2^q)$ is independent of depth while $T_{\text{orig}} = O(2^q \cdot D)$, the ratio $T_{\text{merge}}/T_{\text{orig}}$ decreases as c_{total} (and hence D) grows, steepening the

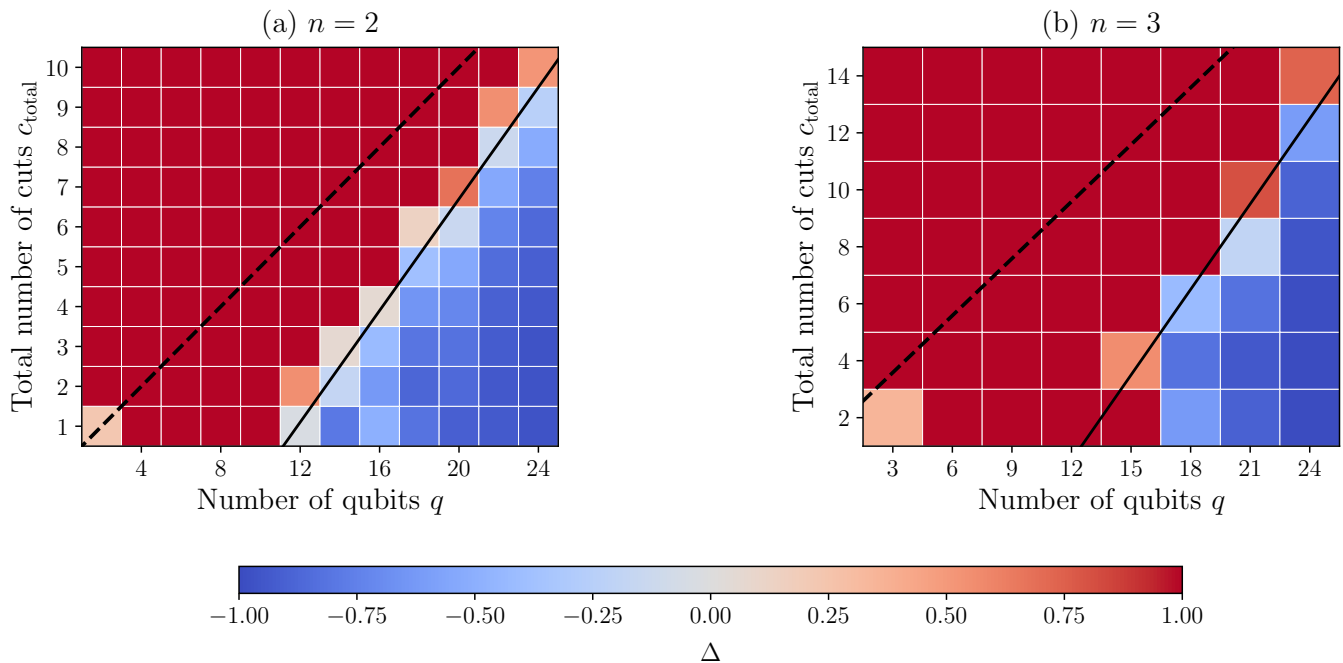


FIG. 2. Measured relative speedup $\Delta = (T_{\text{cut}} - T_{\text{orig}})/T_{\text{orig}}$ on the (q, c_{total}) plane for (a) two-way ($n = 2, q = 2, 4, \dots, 24, c_{\text{total}} = 1, \dots, 10$) and (b) three-way ($n = 3, q = 3, 6, \dots, 24, c_{\text{total}} = 2, 4, \dots, 14$) equal partitioning. Blue indicates speedup ($\Delta < 0$); red indicates slowdown ($\Delta > 0$). The dashed line shows the theoretical threshold derived in Sec. IV. The solid line shows a linear boundary fitted to the measured data by a weighted SVM classifier. Both boundaries confirm that the speedup region grows linearly with q , though the measured boundary is steeper than the theoretical prediction, as discussed in Sec. VB.

measured slope. Meanwhile, $T_{\text{pre}} = O(N_{\text{sub}} D)$ grows much more slowly with q than T_{sub} , contributing a nearly constant offset that lowers the intercept. The linear form $c_{\text{total}} \propto q$ is preserved for both $n = 2$ and $n = 3$, confirming that the theoretical threshold captures the correct scaling.

C. Runtime breakdown and bottleneck crossovers

To identify the dominant cost factors of circuit cutting, we decompose the total cutting time into three phases: preprocessing (T_{pre}), subcircuit simulation (T_{sub}), and merging (T_{merge}). We report these three components as a function of q in Fig. 3 for two-way cutting with $c_{\text{total}} = 6$. Each data point represents the mean of ten independent runs.

For small circuits ($q \lesssim 16$), preprocessing and subcircuit simulation account for most of the total cutting time, while the merging cost is negligible ($< 10^{-1}$ s). However, T_{merge} grows most steeply with q , because the merging step reconstructs the full 2^q -dimensional state vector from the subcircuit results. This leads to two crossover points:

- **First crossover ($q \approx 18$):** T_{merge} surpasses T_{pre} , indicating that merging is no longer a minor overhead relative to preprocessing.

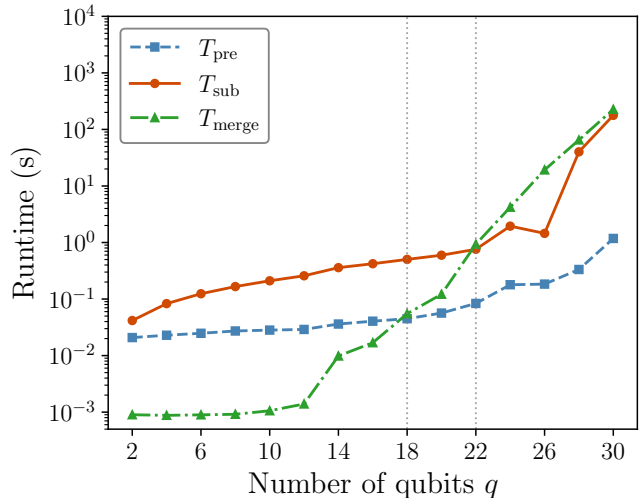


FIG. 3. Runtime breakdown of two-way circuit cutting with $c_{\text{total}} = 6$ cuts, as a function of the number of qubits q . Three phases are shown: preprocessing (T_{pre}), subcircuit simulation (T_{sub}), and merging (T_{merge}). Vertical dotted lines mark the two crossover points: around $q \approx 18$, where merging is no longer a minor overhead relative to preprocessing, and around $q \approx 22$, where merging overtakes subcircuit simulation.

- **Second crossover ($q \approx 22$):** T_{merge} overtakes T_{sub} , becoming the dominant cost among the three

phases. For $q = 30$, merging accounts for approximately 56% of the total cutting time, while subcircuit simulation accounts for 43% and preprocessing is negligible ($< 1\%$).

The same qualitative trend is observed for other cut counts in Fig. 7 in Appendix A.

These crossovers suggest different optimization targets depending on circuit size. For small circuits ($q \lesssim 18$ in our setup), the total cutting time is governed by preprocessing and subcircuit simulation, and standard optimization strategies (e.g. gate fusion, parallel subcircuit simulation) are most effective. For larger circuits ($q \gtrsim 22$ in our setup), optimizing the merging step, for example by employing sparse or compressed state-vector representations [21, 22], yields the greatest reduction in total cutting time.

D. Depth sweep and runtime breakdown

The thresholds in Eqs. (13) and (14) do not contain the circuit depth D , because D cancels in the comparison of T_{sub} with T_{orig} under uniform gate distribution. The speedup boundary is therefore expected to be stable across depths. The depth sweep below tests this expectation empirically.

In practical state-vector simulation, however, the wall-clock time also depends on the circuit depth (or, equivalently, the number of gate applications). To quantify this effect and to assess the robustness of the threshold boundary, we perform a synthetic depth sweep by appending 10^p layers of single-qubit gates (alternating T and X) to the top and bottom qubits of a baseline circuit, while keeping (q, c_{total}) fixed. The circuit diagram is given in Fig. 8 in Appendix A.

We extract the $\Delta = 0$ boundary on the (q, c_{total}) plane for each depth configuration and overlay them in Fig. 4. Specifically, for each depth D we compute $\Delta(q, c_{\text{total}}; D) = (T_{\text{cut}}(q, c_{\text{total}}; D) - T_{\text{orig}}(q; D))/T_{\text{orig}}(q; D)$ and fit a linear decision boundary using a weighted SVM classifier. Cutting is beneficial below each fitted line. The resulting boundaries remain close to one another across all tested depths ($p = 0, 2, 3, 4$), confirming that the speedup–slowdown transition is qualitatively stable. Increasing depth introduces two competing effects: T_{orig} grows with depth, which tends to make the cutting overhead relatively smaller, while T_{sub} also grows with depth, partially offsetting this advantage. These effects largely cancel, so the speedup boundary remains approximately stable. This stability refers to the boundary as a whole. At the level of individual configurations, depth can still tip the balance in favor of cutting, as detailed in Fig. 9 in Appendix A.

To provide an operational guideline, we also estimate the maximum feasible qubit count within a fixed wall-clock budget for both the original simulation and two-way cutting, as shown in Fig. 5. We set the time limit

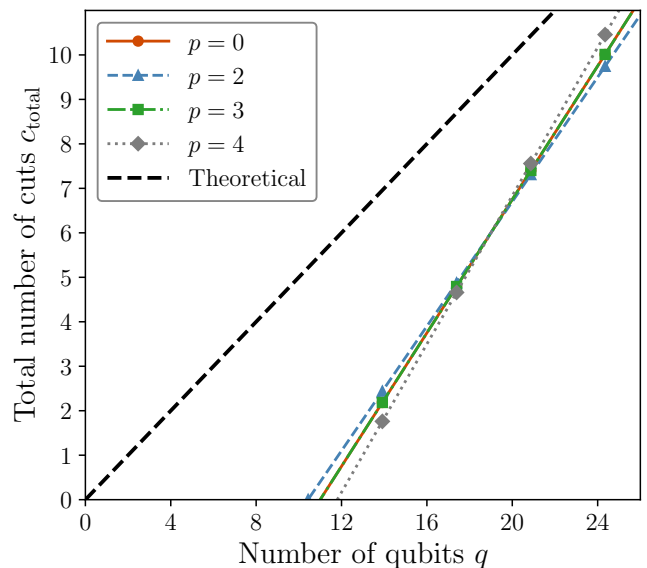


FIG. 4. Speedup boundary on the (q, c_{total}) plane for two-way partitioning ($n = 2$) at four depth configurations ($p = 0, 2, 3, 4$, corresponding to $D \propto 1, 10^2, 10^3, 10^4$ additional gate layers). Each colored line shows the $\Delta = 0$ boundary obtained by a weighted SVM fit at the corresponding depth. Cutting is beneficial below each line. The dashed black line shows the theoretical threshold derived in Sec. IV. The boundaries remain close to one another across all tested depths, confirming that the qubit-count-based threshold provides a reasonable first-order guideline even for circuits of varying depth.

to 10 minutes per simulation run. This time limit was chosen because (i) it is practical for iterative circuit design and verification workflows, and (ii) all reported results are determined entirely from measured simulation times without any extrapolation. Every configuration either completed within the limit or timed out, so the feasibility boundary is exact. Each configuration was executed three independent times. The results were consistent across runs, and the figure reports the mean values. Under this 10-minute budget, the original (uncut) simulation reaches at most 22–26 qubits across all depth configurations ($p = 0, 2, 3, 4$), while two-way cutting extends the feasible range to 28–30 qubits, a gain of 4 to 6 qubits, as indicated by the annotated arrows in Fig. 5. The shaded region highlights the gain from cutting across all depths.

Moreover, the gain increases from 4 to 6 qubits as depth grows from $p = 0$ to $p = 4$, consistent with the observation that T_{cut} grows more slowly with depth than T_{orig} , as shown in Fig. 9 in Appendix A.

E. Scope and limitations

The experiments in this section confirm four qualitative trends within the tested range ($q \leq 24$ for the threshold boundary, $q \leq 30$ for the runtime breakdown): (i) the

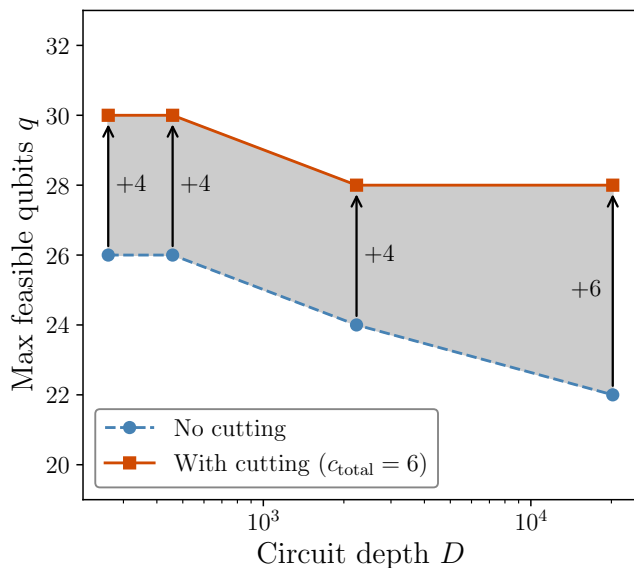


FIG. 5. Maximum feasible qubit count within a 10-minute wall-clock budget, as a function of circuit depth D . The dashed blue line shows the original (uncut) simulation and the solid orange line shows two-way cutting with $c_{\text{total}} = 6$. The shaded region highlights the improvement from cutting. Annotated arrows indicate the qubit-count gain at each depth: 4 qubits for $p = 0, 2, 3$ and 6 qubits for $p = 4$, extending the feasible range from 22–26 (no cutting) to 28–30 (with cutting).

speedup boundary is linear in q , (ii) T_{merge} becomes the dominant cost component at large qubit counts, (iii) the boundary is approximately stable across a wide range of circuit depths, and (iv) circuit cutting extends the feasible simulation range under a fixed wall-clock budget. All four trends originate from the exponential scaling of state-vector simulation and are expected to persist across different platforms and simulator implementations. The quantitative values, however, including the SVM-fitted slopes and intercepts, the bottleneck crossover points, and the feasibility gain, are specific to our single-node environment, benchmark circuit family, and simulator implementation, and should be recalibrated for each target platform. The runtime decomposition methodology and the threshold analysis on the (q, c_{total}) plane are directly applicable to other environments and provide the framework for such recalibration.

The execution times are discussed in terms of circuit depth D following the convention in simulation complexity studies. For sequential gate-application simulators such as Qiskit `Statevector`, the wall-clock time scales with gate count G rather than with D , but the two coincide under the uniform gate distribution assumed in the threshold analysis and in the numerical experiments.

VI. CONCLUSION

We studied the practical conditions under which circuit cutting accelerates classical state-vector simulation with full-state reconstruction. Our main contributions are summarized as follows.

(i) Decomposing the total cutting time into preprocessing, subcircuit simulation, and merging revealed two bottleneck crossovers: merging surpasses preprocessing and then surpasses subcircuit simulation. In our implementation, these crossovers occur around $q \approx 18$ and $q \approx 22$, respectively.

(ii) From this cost model we derived conditions on the maximum cut count c_{total} for which cutting yields a net speedup. The threshold takes the form $c_{\text{total}} \propto q$ and is approximately depth-independent. State-vector experiments up to 24 qubits confirm the predicted threshold.

(iii) As a practical illustration, we estimated the maximum feasible qubit count under a 10-minute wall-clock budget. Two-way cutting extends this limit by 4 to 6 qubits compared to simulation without cutting, with the gain increasing at larger depths.

These results also offer a perspective on the well-known 49-qubit barrier for state-vector simulation [10]. Circuit cutting does not unconditionally break this barrier, because the exponential overhead in cut count implies that only circuits requiring a small number of cuts can achieve a net speedup. However, the threshold conditions provide a practical pre-screening criterion: given a circuit’s (q, c_{total}) parameters, one can determine in advance whether cutting is likely to yield a net speedup, without committing to the full simulation.

The experimental validation covers $q \leq 24$ for the threshold boundary and $q \leq 30$ for the runtime breakdown. Beyond this range, the threshold predictions rely on extrapolation of the order-of-magnitude scaling, and memory constraints become the practical bottleneck for single-node state-vector simulation. The quantitative crossover points and feasibility gains reported here are specific to our single-node environment and should be recalibrated for each target platform. The functional form of the threshold and the regime structure are expected to persist across different environments.

This work focuses on full-state reconstruction, where the $O(2^q)$ merging cost is unavoidable. When only expectation values are needed, the merging phase can be replaced by classical summation of subcircuit expectation values, which eliminates the $O(2^q)$ cost and changes the regime structure. Extending the present framework to that setting is a natural next step.

Several further directions remain open. First, the threshold model can be refined by extending to asymmetric and topology-aware partitioning, and the effective threshold can be further relaxed by parallel subcircuit execution and more efficient merging algorithms. Second, applying this framework to application-specific circuits, such as those arising in quantum chemistry and combinatorial optimization, would enable practical pre-screening

of whether circuit cutting yields a net speedup in realistic workflows. Third, incorporating quantum execution costs, including shot count and state tomography overhead, would extend the analysis to a quantum-classical crossover regime. This requires a separate cost model for the quantum side and is left for future work.

ACKNOWLEDGMENTS

This paper is based on results obtained from a project, JPNP23003, commissioned by the New Energy and Industrial Technology Development Organization (NEDO). The authors would like to thank Junya Nakamura, Tsuyoshi Kitano, Hana Ebi, Hideaki Kawaguchi, Takaharu Yoshida, Hiroki Kuji and Shigetora Miyashita for their fruitful discussions. TS is supported by JST Grant Number JPMJPF2221.

APPENDIX A: SUPPLEMENTARY FIGURES

This appendix collects supporting visualizations that provide additional evidence for the claims in the main text. It covers equal-partitioning optimality, runtime breakdown across cut counts, and depth-sweep details.

1. Optimality of equal partitioning

We verify that equal partitioning minimizes the total simulation time. A 20-qubit circuit is partitioned into two subcircuits by varying the number of qubits in the upper subcircuit from 1 to 19. For each configuration, the simulation time is measured 20 times and the mean and standard deviation are computed for 1 to 5 cuts. As shown in Fig. 6, the simulation time ratio is minimized when the circuit is divided into equal halves ($q/2 = 10$ qubits per subcircuit).

2. Runtime breakdown across cut counts

The runtime breakdown for two-way cutting at four representative cut counts ($c = 3, 6, 9, 12$) is shown in Fig. 7, including the $c = 6$ case in Fig. 3. The same qualitative trend as in Fig. 3 is observed across all cut counts: T_{merge} grows most steeply with q , producing two crossover points similar to those identified in Sec. V C. As c increases, the crossover points shift slightly toward larger q , but the overall structure of the runtime breakdown remains unchanged.

3. Depth sweep: circuit and runtime breakdown

The depth-augmented circuit used in the depth sweep of Sec. V D is shown in Fig. 8. 10^p layers of alternating T

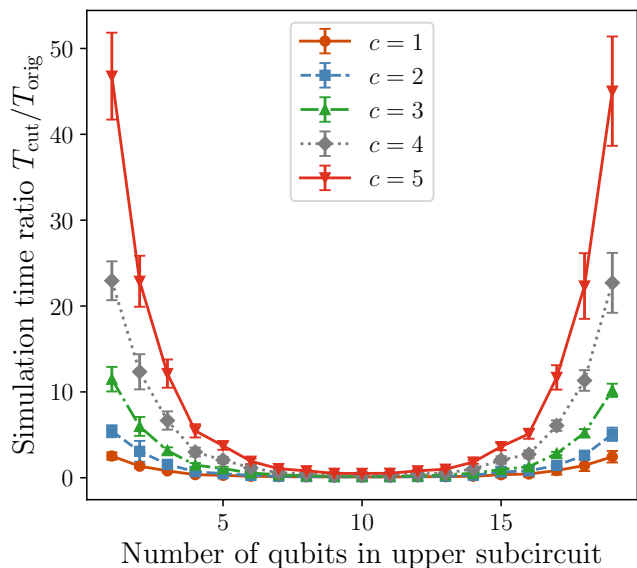


FIG. 6. Simulation time ratio $T_{\text{cut}}/T_{\text{orig}}$ as a function of the number of qubits in the upper subcircuit for a 20-qubit circuit partitioned into two subcircuits with $c = 1, \dots, 5$ cuts. The minimum occurs at $q/2 = 10$ for all cut counts, confirming that equal partitioning minimizes the total simulation time.

and X gates are appended to the top and bottom qubits of the baseline circuit, while the number of qubits q and cuts c are kept fixed.

We report the runtime breakdown $\{T_{\text{pre}}, T_{\text{sub}}, T_{\text{merge}}\}$ as a function of circuit depth D for a representative configuration ($q = 24$, $c = 10$, two-way partitioning) in Fig. 9. Among the three components, T_{pre} and T_{sub} grow approximately linearly with D , whereas T_{merge} is approximately depth-independent. As a result, the dominant component within T_{cut} shifts from T_{merge} to T_{sub} around $D \approx 750$. Because T_{merge} does not grow with depth, T_{cut} grows more slowly than T_{orig} , and T_{orig} overtakes T_{cut} around $D \approx 3000$.

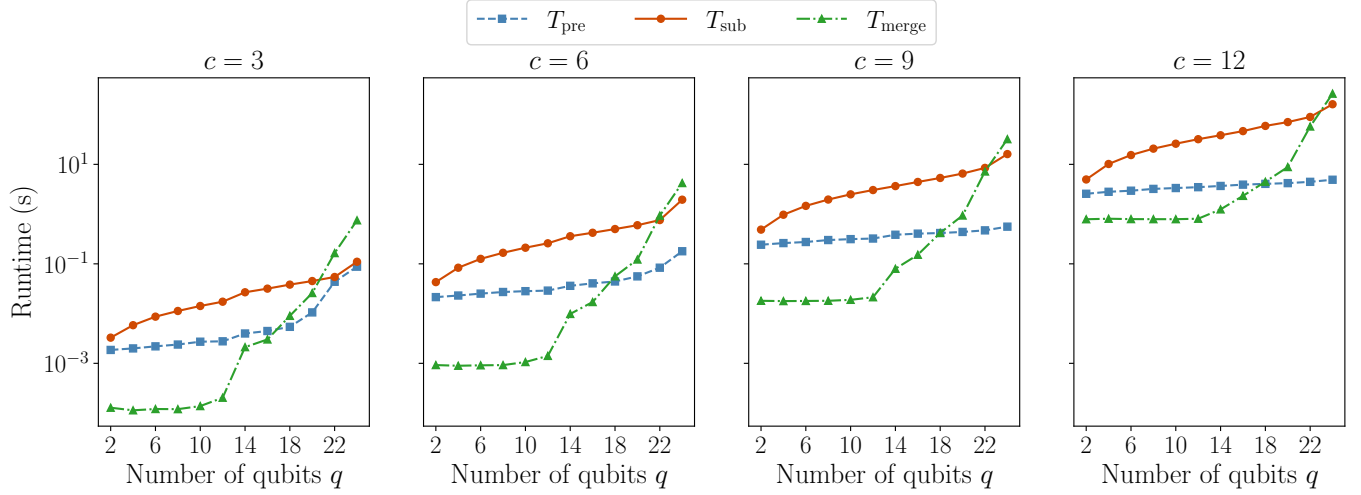


FIG. 7. Runtime breakdown of two-way cutting ($n = 2$) for four representative cut counts $c = 3, 6, 9, 12$. Each panel shows the three cost components: preprocessing (T_{pre}), subcircuit simulation (T_{sub}), and merging (T_{merge}) as a function of the number of qubits q . The same qualitative trend as in Fig. 3 is observed across all cut counts: T_{merge} grows most steeply with q , producing two crossover points similar to those identified in Sec. V C. The $c = 6$ panel corresponds to Fig. 3 in the main text and is included for ease of comparison.

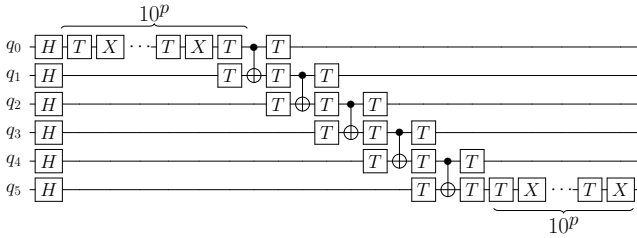


FIG. 8. Depth-augmented circuit used in the depth sweep. 10^p layers of alternating T and X gates are appended to the top and bottom qubits of the baseline circuit. The number of qubits q and cuts c are kept fixed while only the circuit depth is varied.

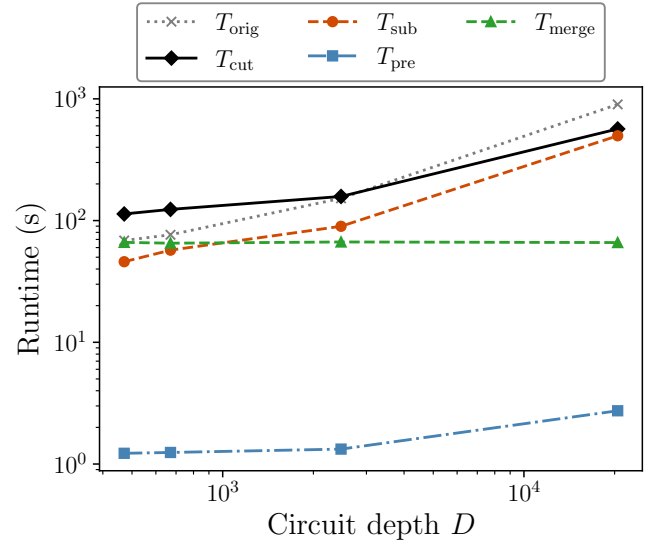


FIG. 9. Runtime breakdown as a function of circuit depth D for a 24-qubit circuit with 10 cuts, divided into 2 segments. The total cutting time (T_{cut}) is primarily composed of the subcircuit simulation time (T_{sub}), and both exhibit a similar scaling trend with depth. In contrast, the merging overhead (T_{merge}) remains approximately constant, while the preprocessing cost (T_{pre}) shows a weaker dependence on depth. Around $D \approx 750$, the dominant bottleneck within T_{cut} shifts from T_{merge} to T_{sub} . The original simulation time without cutting (T_{orig}) grows faster than T_{cut} and overtakes it around $D \approx 3000$, indicating that circuit cutting can become advantageous at sufficient depth, even for configurations that do not yield speedup at small depth.

APPENDIX B: PSEUDOCODE AND COMPUTATIONAL COST

This appendix provides the pseudocodes underlying the cost expressions in Table I. All pseudocodes assume CZ gate cutting with $k = 2$. In the preprocessing phase (Algorithm 1), each CX gate at a partition boundary is first converted to CZ via $CX = (I \otimes H) CZ (I \otimes H)$ and then decomposed.

Algorithm 1 Preprocessing

Input: Original circuit \mathcal{C} on q qubits, partition $\{G_1, \dots, G_n\}$ of qubits

Output: Subcircuits $\{S_i^{(r)}\}$ for segment $i = 1, \dots, n$ and decomposition index $r = 1, \dots, 2^{c_i}$, where c_i is the total number of cuts on all boundaries adjacent to segment i . Merge index table \mathcal{M} .

```

1: Scan  $\mathcal{C}$  and identify all CX gates that straddle partition boundaries
2: for each segment  $i = 1, \dots, n$  do
3:   Split  $\mathcal{C}$  at each boundary gate into gate-list fragments  $F_i^{(0)}, F_i^{(1)}, \dots, F_i^{(c_i)}$  restricted to qubits in  $G_i$ 
4:   for each combination  $\mathbf{b} \in \{0, 1\}^{c_i}$  do
5:      $S_i^{(\mathbf{b})} \leftarrow F_i^{(0)}$ 
6:     for  $j = 1, \dots, c_i$  do
7:       if  $b_j = 0$  then
8:         Append  $HSH$  (or  $S$ ) gate to cut qubit
9:       else
10:        Append  $HS^\dagger H$  (or  $S^\dagger$ ) gate to cut qubit
11:       end if
12:       Append fragment  $F_i^{(j)}$ 
13:     end for
14:   end for
15: end for
16: Build merge index table  $\mathcal{M}$  mapping each global combination index to the per-segment indices  $\mathbf{b}$ 

```

Complexity. Time: $O(N_{\text{sub}} \cdot D)$, where $N_{\text{sub}} = \sum_{i=1}^n 2^{c_i}$ is the total number of subcircuits. When every boundary has the same number of cuts c , edge segments have $c_i = c$, interior segments have $c_i = 2c$, and $N_{\text{sub}} = 2 \cdot 2^c$ for $n = 2$. Memory: $O(N_{\text{sub}} \cdot D)$.

Algorithm 2 Subcircuit simulation

Input: Subcircuits $\{S_i^{(r)}\}$ from Algorithm 1

Output: State vectors $\{|\psi_i^{(r)}\rangle\}$, each of dimension 2^{q_i}

```

1: for each segment  $i = 1, \dots, n$  do
2:   for each decomposition index  $r = 1, \dots, 2^{c_i}$  do
3:      $|\psi_i^{(r)}\rangle \leftarrow \text{StateVectorSimulate}(S_i^{(r)}) \triangleright O(2^{q_i} D_{\text{seg},i})$ 
4:   end for
5: end for

```

Complexity. Time: $O(\sum_{i=1}^n 2^{c_i} \cdot 2^{q_i} \cdot D_{\text{seg},i})$, where q_i is the number of qubits and $D_{\text{seg},i}$ is the depth of segment i (e.g. $O(2 \cdot 2^c \cdot 2^{q/2} \cdot D_{\text{seg}})$ for equal bipartition with c cuts). Memory: $O(2^{q_{\text{max}}})$ per subcircuit, up to $O(N_{\text{sub}} \cdot 2^{q_{\text{max}}})$ if all state vectors are retained for merging, where $q_{\text{max}} = \max_i q_i$.

Algorithm 3 Merging

Input: State vectors $\{|\psi_i^{(r)}\rangle\}$ from Algorithm 2, merge index table \mathcal{M}

Output: Reconstructed full state vector $|\Psi\rangle$ of dimension 2^q

```

1: Compute  $\{\alpha_m\}$  from CZ decomposition  $\triangleright O(2^{c_{\text{max}}})$ 
2:  $|\Psi\rangle \leftarrow \mathbf{0}_{2^q}$ 
3: for each combination  $m = 1, \dots, 2^{c_{\text{max}}}$  do
4:   Look up per-segment indices  $(r_1, \dots, r_n) \leftarrow \mathcal{M}[m]$ 
5:    $|\phi_m\rangle \leftarrow |\psi_1^{(r_1)}\rangle \otimes \dots \otimes |\psi_n^{(r_n)}\rangle \triangleright O(2^q)$ 
6:    $|\Psi\rangle \leftarrow |\Psi\rangle + \alpha_m |\phi_m\rangle \triangleright O(2^q)$ 
7: end for

```

Complexity. Time: $O(2^{c_{\text{max}}} \cdot 2^q)$, where $c_{\text{max}} = \max_i c_i$ ($2^{c_{\text{max}}}$ tensor products, each producing a 2^q -dimensional vector; e.g. $O(2^c \cdot 2^q)$ for $n = 2$). Memory: $O(2^q)$ (one accumulator vector $|\Psi\rangle$ and one temporary vector $|\varphi_m\rangle$).

-
- [1] J. M. Shalf and R. Leland, Computing beyond Moore's law, *Computer* **48**, 14 (2015).
 - [2] J. Preskill, Quantum Computing in the NISQ era and beyond, *Quantum* **2**, 79 (2018), arXiv:1801.00862 [quant-ph].
 - [3] S. Bravyi, G. Smith, and J. A. Smolin, Trading classical and quantum computational resources, *Physical Review X* **6**, 021043 (2016).
 - [4] T. Peng, A. W. Harrow, M. Ozols, and X. Wu, Simulating large quantum circuits on a small quantum computer, *Phys. Rev. Lett.* **125**, 150504 (2020), arXiv:1904.00102 [quant-ph].
 - [5] K. Mitarai and K. Fujii, Constructing a virtual two-qubit gate by sampling single-qubit operations, *New J. Phys.* **23**, 023021 (2021), arXiv:1909.07534 [quant-ph].
 - [6] L. Brenner, C. Piveteau, and D. Sutter, Optimal wire cutting with classical communication (2023), arXiv:2302.03366 [quant-ph].
 - [7] H. Harada, K. Wada, and N. Yamamoto, Doubly optimal parallel wire cutting without ancilla qubits, *PRX Quantum* **5**, 040308 (2024), arXiv:2303.07340 [quant-ph].
 - [8] I. L. Markov, A. Fatima, S. V. Isakov, and S. Boixo, Quantum supremacy is both closer and farther than it appears (2018), arXiv:1807.10749 [quant-ph].
 - [9] F. Pan, K. Chen, and P. Zhang, Solving the sampling problem of the Sycamore quantum circuits, *Phys. Rev. Lett.* **129**, 090502 (2022), arXiv:2111.03011 [quant-ph].
 - [10] E. Pednault, J. A. Gunnels, G. Nannicini, L. Horesh, T. Magerlein, E. Solomonik, and R. Wisnieff, Breaking the 49-qubit barrier in the simulation of quantum circuits

- (2017), arXiv:1710.05867 [quant-ph].
- [11] W. Tang, T. Tomesh, M. Suchara, J. Larson, and M. Martonosi, Cutqc: Using small quantum computers for large quantum circuit evaluations, in *Proceedings of the 26th ACM International Conference on Architectural Support for Programming Languages and Operating Systems (ASPLOS '21)* (2021).
- [12] T. Jones, A. Brown, I. Bush, and S. C. Benjamin, Quest and high performance simulation of quantum computers, *Scientific Reports* **9**, 10736 (2019).
- [13] B. Villalonga, S. Boixo, B. Nelson, C. Henze, E. Rieffel, R. Biswas, and S. Mandrà, A flexible high-performance simulator for verifying and benchmarking quantum circuits implemented on real hardware (2018), arXiv:1811.09599 [quant-ph].
- [14] Y. Suzuki, S. Uno, R. Raymond, T. Tanaka, T. Onodera, and N. Yamamoto, Qulacs: a fast and versatile quantum circuit simulator for research purpose, *Quantum* **5**, 559 (2021).
- [15] T. Nguyen, D. Lyakh, E. Dumitrescu, D. Clark, J. Larkin, and A. McCaskey, Tensor network quantum virtual machine for simulating quantum circuits at exascale (2021), arXiv:2104.10523 [quant-ph].
- [16] F. Arute *et al.*, Quantum supremacy using a programmable superconducting processor, *Nature* **574**, 505 (2019).
- [17] L. Schmitt, C. Piveteau, and D. Sutter, Cutting circuits with multiple two-qubit unitaries, *Quantum* **9**, 1634 (2025).
- [18] A. Lowe, M. Medvidović, A. Hayes, L. J. O’Riordan, T. R. Bromley, J. M. Arrazola, and N. Killoran, Fast quantum circuit cutting with randomized measurements, *Quantum* **7**, 934 (2023), arXiv:2207.14734 [quant-ph].
- [19] S. Balakrishnan and R. Sankaranarayanan, Operator-Schmidt decomposition and the geometrical edges of two-qubit gates, *Quantum Information Processing* **10**, 449 (2011).
- [20] S. C. Marshall, C. Gyurik, and V. Dunjko, High dimensional quantum machine learning with small quantum computers, *Quantum* **7**, 1078 (2023), arXiv:2203.13739 [quant-ph].
- [21] N. Huffman, D. Pavlichin, and T. Weissman, Lossy compression for schrödinger-style quantum simulations (2024), arXiv:2401.11088 [quant-ph].
- [22] X.-C. Wu, S. Di, F. Cappello, H. Finkel, Y. Alexeev, and F. T. Chong, Amplitude-aware lossy compression for quantum circuit simulation (2018), arXiv:1811.05140 [quant-ph].
- [23] I. L. Markov and Y. Shi, Simulating quantum computation by contracting tensor networks, *SIAM Journal on Computing* **38**, 963 (2008).
- [24] A. Peruzzo, J. McClean, P. Shadbolt, M.-H. Yung, X.-Q. Zhou, P. J. Love, A. Aspuru-Guzik, and J. L. O’Brien, A variational eigenvalue solver on a photonic quantum processor, *Nat. Commun.* **5**, 4213 (2014).
- [25] A. Kandala, A. Mezzacapo, K. Temme, M. Takita, M. Brink, J. M. Chow, and J. M. Gambetta, Hardware-efficient variational quantum eigensolver for small molecules and quantum magnets, *Nature* **549**, 242 (2017).
- [26] E. Farhi, J. Goldstone, and S. Gutmann, A quantum approximate optimization algorithm (2014), arXiv:1411.4028 [quant-ph].
- [27] A. M. Childs, Y. Su, M. C. Tran, N. Wiebe, and S. Zhu, Theory of Trotter error with commutator scaling, *Phys. Rev. X* **11**, 011020 (2021).